

High-Voltage Single-Ion Covalent Organic Framework Electrolytes Enabled by Nitrile Migration Ladders for Lithium Metal Batteries

Weiping Li, Shantao Han, Chenxi Xiao, Jingying Yan, Baifei Wu, Peng Wen, Jun Lin,
Mao Chen, and Xinrong Lin*

Abstract: The poor electrochemical stability window and low ionic conductivity in solid-state electrolytes hinder the development of safe, high-voltage, and energy-dense lithium metal batteries. Herein, taking advantage of the unique electronic effect of nitrile groups, we designed a novel azanide-based single-ion covalent organic framework (CN-iCOF) structure that possesses effective Li^+ transport and high-voltage stability in lithium metal batteries. Density functional theory (DFT) calculations and molecular dynamics (MD) revealed that electron-withdrawing nitrile groups not only resulted in an ultralow HOMO energy orbital but also enhanced Li^+ dissociation through charge delocalization, leading to a high t_{Li^+} of 0.93 and remarkable oxidative stability up to 5.6 V (vs. Li^+/Li) simultaneously. Moreover, cyanation leveraging Strecker reaction transformed reversible imine-linkage to a stable sp^3 -carbon-containing azanide anion, which facilitated contorted alignment of transport “ladders” along the one-dimensional anionic channels and the ionic conductivity could reach $1.33 \times 10^{-5} \text{ S cm}^{-1}$ at ambient temperature without any additives. As a result, CN-iCOF allowed operation of solid-state lithium metal batteries with high-voltage cathodes such as $\text{LiNi}_{0.8}\text{Mn}_{0.1}\text{Co}_{0.1}\text{O}_2$ (NCM811), demonstrating stable lithium deposition up to 1,100 h and reversible battery cycling at ambient temperature up to 4.5 V, shedding light on the importance of discovering new functionality for forthcoming high-performance batteries.

Introduction

Lithium battery technology has been a key enabler in widespread applications including portable electronics, elec-

tric cars and grid-scale storage.^[1] As current lithium-ion batteries with graphite anodes are insufficient to keep pace with the growing demand in energy density, there is an urgent demand to unleash the power of Li metal-based anode that offers ultrahigh specific capacity (3,860 mAh g⁻¹) and low reduction potential (-3.04 V vs. standard hydrogen electrode) to develop lithium metal batteries (LMBs).^[2] Together with the promising solid-state electrolytes that could eliminate battery safety concerns and increase energy density at the system level,^[3] the energy densities of solid-state LMBs are projected to be doubled to >500 Wh kg⁻¹.^[4] So far, ceramic and polymer electrolytes represent the two most important categories of solid-state electrolytes.^[5] However, accelerating ion transport kinetics in these two systems are at the expense of interfacial stability and/or mechanical strength.^[6] Meanwhile, few state-of-the-art solid-state electrolytes that are compatible with Li metal anode can withstand high cut-off voltages and work with Ni-rich cathodes such as $\text{LiNi}_{0.8}\text{Mn}_{0.1}\text{Co}_{0.1}\text{O}_2$ (NCM811),^[7] compromising accessible energy density. Therefore, increasing oxidative stability of solid-state electrolytes in lithium-metal batteries while achieving efficient ion transport remains a significant challenge.

Crystalline porous materials such as covalent organic frameworks (COFs) have garnered considerable attention as a novel class of solid-state electrolytes because of their periodical crystalline structure with flexible chemical tunability, which could provide ionic conduction in the highly ordered channels.^[8] Beyond crystalline porous materials, an attractive approach to enhance Li^+ transport is the concept of “single-ion” conductors, which immobilize the anions on the bulky electrolyte backbones^[9] and thus yield high Li^+ transference number (t_{Li^+}) and mitigate transport-related polarization,^[10] increasing the operating voltage of the cell and suppressing undesired interfacial growth of dendritic lithium. Recently, important advances have been made in developing imidazolate, sulfonate, and carbonate-based single-ion COFs,^[11] in addition to single-ion conducting polymers^[12] and metal-organic frameworks (MOFs)^[13] as emerging solid-state electrolytes. However, despite of showing electrochemical stability and promising t_{Li^+} in the range of 0.36 to 0.90, structural reversibility in COF electrolytes could lead to low operating voltage for single-ion COF electrolytes.^[14] In addition, transport of Li^+ ions between the anionic frameworks might be hindered without effective driving force for Li^+ migration. To date, single-ion COF electrolytes with enhanced Li^+ transport and oxidative stability that operate at ambient temperature and elevated

[*] W. Li, C. Xiao, J. Yan, B. Wu, Prof. Dr. X. Lin

Department Division of Natural and Applied Sciences, Duke Kunshan University, Kunshan, Jiangsu, 215306, China
E-mail: xl422@duke.edu

W. Li, C. Xiao, J. Yan, B. Wu, Prof. Dr. J. Lin, Prof. Dr. X. Lin
School of Chemical Science and Technology, Yunnan University, Kunming, 650091, China

S. Han, P. Wen, Prof. Dr. M. Chen
State Key Laboratory of Molecular Engineering of Polymers, Department of Macromolecular Science, Fudan University, Shanghai, 200433, China

voltages above 4.3 V to achieve high energy density lithium metal batteries, have not been reported.

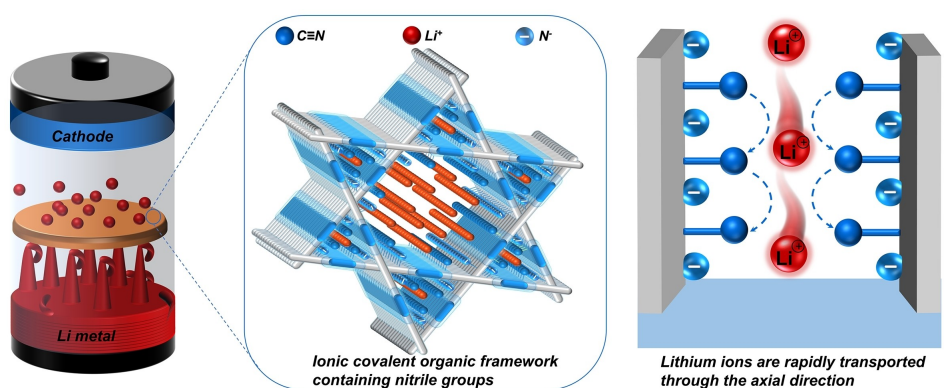
Herein, we develop a novel single-ion conducting COF (iCOF) electrolyte that is high-voltage stable in lithium metal batteries. Converting the reversible imine-based linkage to a stable α -aminonitrile linkage leveraging Strecker reaction,^[15] CN-iCOF bearing azanide-based anionic centers adjacent to strongly electron-withdrawing nitrile groups were generated followed by deprotonation. Density functional theory (DFT) calculations and molecular dynamics (MD) simulations elucidated the fundamental effect of nitrile groups in not only lowering the HOMO energy orbital but also enhancing Li^+ dissociation through charge delocalization, resulting in a high t_{Li^+} of 0.93 and remarkable oxidative stability up to 5.6 V (vs. Li^+/Li) in single-ion COF electrolytes. Moreover, the tetrahedral geometry of sp^3 -carbon-based linkage allows a unique contorted alignment of nitrile transport “ladders” along the one-dimensional anionic channels aided by Li^+-CN coordination (Scheme 1), facilitating axial Li^+ migration between the vertically stacked frameworks and offering energetically favored transport. Accordingly, the resultant single-ion COF exhibits high ionic conductivity of $1.33 \times 10^{-5} \text{ S cm}^{-1}$ at 30°C and low activation energy (E_a) of 0.20 eV without additional lithium salts or solvents, while maintaining a strong mechanical modulus of 9.6 GPa. Finally, assembled lithium metal batteries showed prolonged dendrite-free Li plating/stripping behavior and reversible charge–discharge cycling up to 4.5 V coupled with high-voltage cathodes, shedding light on novel molecular design of porous crystalline ion conductors for high-performance lithium battery technologies.

Results and Discussion

To prepare the high-performance single-ion CN-iCOF electrolyte, we designed a three-step synthesis to transform from the reversible imine-linked Im-COF, to stable aminonitrile-linked CN-COF intermediate, and subsequently to the nitrile-containing single-ion CN-iCOF. Specifically, we first carried out condensation between 4, 4', 4'', 4'''-(ethene-1, 1, 2, 2-tetrayl)tetraaniline (ETTA) and 2, 3, 5, 6-

tetrafluoroterephthalaldehyde (TFTA) under solvothermal conditions to synthesize Im-COF (Scheme S1 and Table S1). Fluorinated aldehyde of TFTA was selected as one of the building blocks for the favorable stabilizing effect offered by fluorination in electrolyte materials.^[16] ETTA monomer was chosen to form a novel structure of COF material with TFTA. In the following step, irreversible α -aminonitrile linkage was formed via Strecker reaction employing toluene, $\text{BF}_3\text{-OEt}_2$, and trimethylsilyl cyanide, introducing the electron-withdrawing nitrile groups ($\text{C}\equiv\text{N}$) on the carbon that is adjacent to the amino groups (Scheme S2). Finally, the resulted CN-COF was subjected to a deprotonation reaction on amino groups with a butyl lithium reagent ($n\text{-BuLi}$, 1.6 M in hexane), leading to lithiated CN-iCOF as a single-ion conducting COF electrolyte material (Figure 1a and Scheme S3).

The stepwise structural transformations from Im-COF, CN-COF to single-ion CN-iCOF were supported by comprehensive characterizations including solid-state ^{13}C cross-polarization magic angle spinning (CP/MAS), Fourier-transform infrared spectroscopy (FT-IR), X-ray photoelectron spectroscopy (XPS) and powder X-ray diffraction (PXRD). As shown in Figure 1b, in Im-COF, only sp^2 carbons above 100 pm were observed, with the imine signal identified at around 150–160 ppm. In both CN-COF (Figure S1) and CN-iCOF (Figure 1b), while the aromatic ^{13}C peaks were found around 100–155 ppm, the peak corresponding to the sp^3 carbon next to the nitrile groups appeared at approximately 41 ppm. Additionally, lack of aldehyde carbon peaks around 190–200 ppm in all three COFs indicated the complete conversion of the monomers.^[17] The Fourier transform infrared (FT-IR) spectra of Im-COF showed formation of imine ($\text{C}\equiv\text{N}$) peaks at 1617 cm^{-1} compared with that of carbonyl group ($\text{C}=\text{O}$) in aldehyde (Figure 1c). For CN-COF, the characteristic peaks at 3350 cm^{-1} ($\text{N}-\text{H}$) and 1515 cm^{-1} ($\text{C}-\text{N}$), together with a weak peak at 2251 cm^{-1} ($\text{C}\equiv\text{N}$), indicated the existence of an α -aminonitrile moiety (Figure S2).^[10b] Subsequently, the XPS spectra further affirmed the formation of α -aminonitrile-linked CN-COF. The high-resolution C 1s XPS spectra reveal the peaks at 285.9 eV and 285.5 eV (Figure S3–S4), which are attributed respectively to the



Scheme 1. Schematic of single-ion COF electrolytes with nitrile “ladders” facilitating ion transport and high voltage tolerance.

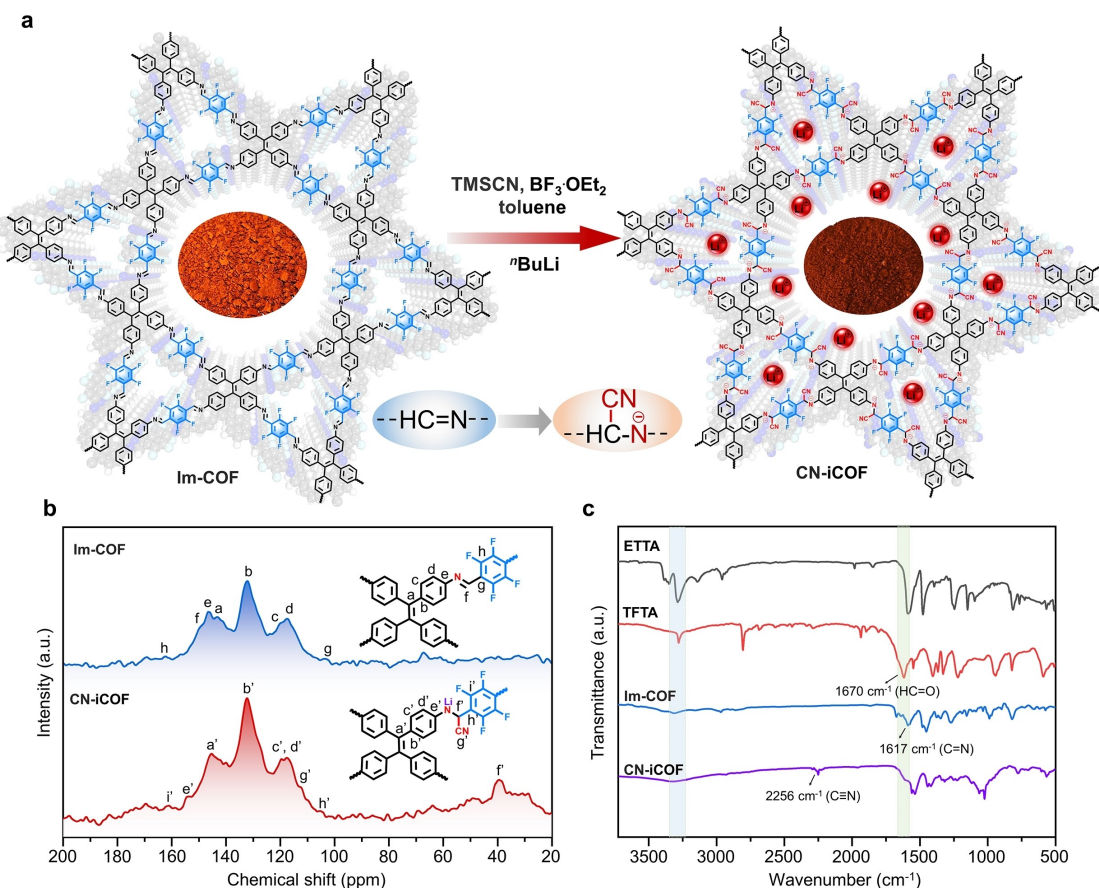


Figure 1. a) Synthesis of CN-iCOF by Strecker reaction of Im-COF and post-modification. b) Solid-state CP/MAS ^{13}C NMR spectra of Im-COF and CN-iCOF. c) Fourier-transform infrared spectroscopy (FT-IR) spectra of ETTA, TFTTA, Im-COF and CN-iCOF.

$\text{C}=\text{N}-\text{C}$ bonds (in Im-COF) and the $\text{C}\equiv\text{N}$ bonds (in CN-COF and CN-iCOF). Additionally, the characteristic peaks of N 1s at 399.2 and 402.0 eV associated with the $-\text{CN}$ and $\text{Ph}-\text{NH}-\text{CH}(\text{CN})\text{Ph}$ moieties in CN-COF and CN-iCOF were clearly observed (Figure 2a).^[17] After the deprotonation reaction, the N 1s peak shifted to 401.5 eV, indicating the formation of $\text{Ph}-\text{NLi}-\text{CH}(\text{CN})\text{Ph}$. In addition, in CN-iCOF, ^7Li NMR showed a singlet at 0.11 ppm, confirming the successful lithiation to form a single-ion Li^+ conducting COF material (Figure 2b). Furthermore, the amount of Li^+ ions counteracting the covalently immobilized anions in the single-ion COF framework was quantified by inductively coupled plasma optical emission spectroscopy (ICP-OES), which revealed the presence of 2.9 wt % elemental Li (Figure S5), agreeing well with the calculated value.

The crystal structures of Im-COF, CN-COF, and CN-iCOF were characterized by powder X-ray diffraction (PXRD). As shown in Figure 2c, the PXRD pattern of Im-COF displayed a series of distinct peaks 2.65°, 4.54°, 5.23°, 6.94°, 7.85°, 9.46°, and 10.47°, corresponding to the (100), (110), (200), (210), (300), (310), and (400) crystal planes, respectively.^[18] After lithiation, the framework of CN-iCOF was not changed, and similar PXRD peaks as those in CN-COF were observed in the experimental pattern of

CN-iCOF (Figure 2d), suggesting the stable architecture of CN-iCOF. With optimized structure, AA and staggered AB stacking modes were generated. CN-iCOF adopted the AA stacking mode as opposed to staggered AB stacking (Figure S6–S8), as indicated by the negligible difference between the simulated and experimental patterns (Figure 2d, black and red curve). The Pawley refinement also led to a space group of P6 with $a=b=39.21 \text{ \AA}$, $c=5.06 \text{ \AA}$, $\alpha=\beta=90^\circ$ and $\gamma=120^\circ$, and R_p and R_{wp} values of 2.24 and 1.67 %, respectively (Table S2–S4). The porosity of Im-COF, CN-COF, and CN-iCOF was determined through nitrogen gas sorption isotherm at 77 K. The specific surface areas calculated according to the Brunauer–Emmett–Teller (BET) model were 1002, 600, and $300 \text{ m}^2 \text{ g}^{-1}$, respectively (Figure 2e–2f, Figure S9–S10). The decrease in specific surface area from Im-COF to CN-iCOF was attributed to an increase in framework mass and reduction in pore volume. The pore size distribution of CN-iCOF was found to be centered at 14.3 Å and 29.2 Å (vs. that of 13.7 Å and 29.4 Å in Im-COF), indicating a distinctive bimodal pore feature. Change of morphology from nanoflower clusters in Im-COF to nanospheroids in CN-iCOF was observed via field emission scanning electron microscopy (FE-SEM, Figure 2g and S11), and energy dispersive spectrometer (EDS) spectra of CN-iCOF exhibited a uniform distribution of C, N, F

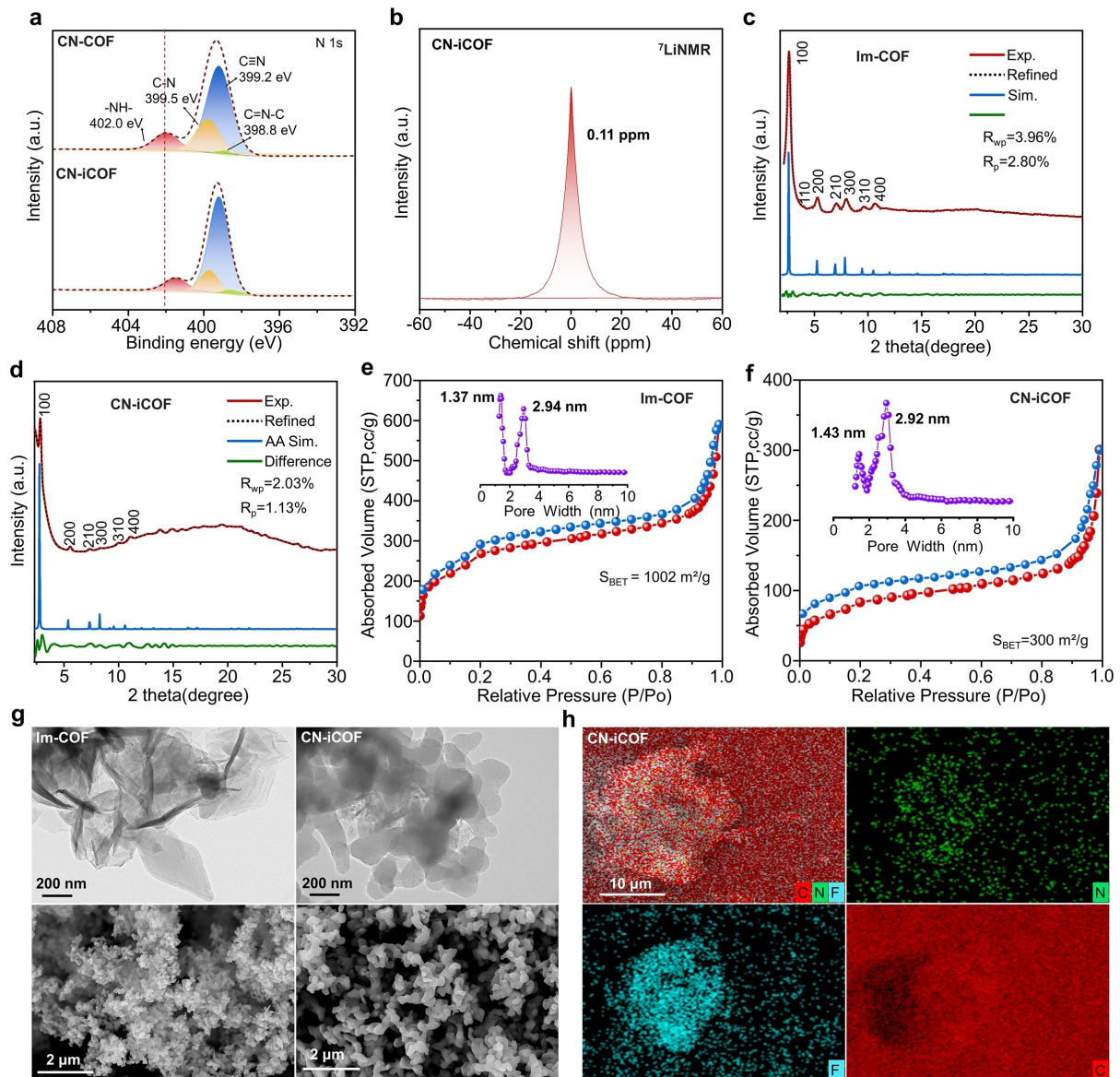


Figure 2. a) Comparison of N 1s XPS spectrum of CN-COF and CN-iCOF. b) Solid-state CP/MAS ^7Li NMR spectra of CN-iCOF. c-d) PXRD patterns of Im-COF and CN-iCOF, with simulated patterns for eclipsed AA stacking mode (blue line) and the refinement differences (green line). e-f) Nitrogen gas adsorption isotherms for Im-COF and CN-iCOF. Insets are the pore size distribution calculated after fitting DFT models to adsorption data. g) TEM and SEM images of Im-COF and CN-iCOF. h) Elemental mapping of CN-iCOF by EDS.

elements (Figure 2h). Additionally, thermogravimetric analysis (TGA) indicated that Im-COF, CN-COF, and CN-iCOF showed no significant weight loss until approximately 300°C, showing similar thermal stability as other single-ion COFs (Figure S12).

To evaluate the role of strongly electron-withdrawing nitrile groups on the electrochemical stability of the prepared single-ion CN-iCOF, the energies of the lowest unoccupied molecular orbital (LUMO) and the highest occupied molecular orbital (HOMO) were calculated by DFT calculations. For more direct comparison, the molecular fragments without nitrile groups (M1) and with nitrile groups (M2) were examined. As shown in Figure 3a, the incorporation of nitrile effectively lowered the HOMO of

M2 (-6.39 eV) compared with M1 (-5.81 eV), indicating higher oxidative stability of M2. Furthermore, the energy band gap (E_g) between the HOMO and LUMO levels of M2 (5.12 eV) was significantly higher than that of M1 (4.85 eV), suggesting that M2 is more suitable as a solid-state electrolyte that needs to be ionically conductive yet electronic insulating. Linear sweep voltammetry (LSV) was performed to experimentally characterize the electrochemical window of the prepared single-ion COFs. Of note, CN-iCOF with inherent lithiation was used as the electrolyte itself without need to further add lithium salts, while neutral COF such as Im-COF were investigated with additional incorporation of lithium salts. It can be seen that the electrochemical stability window of CN-iCOF was approximately 5.6 V (Figure 3b),

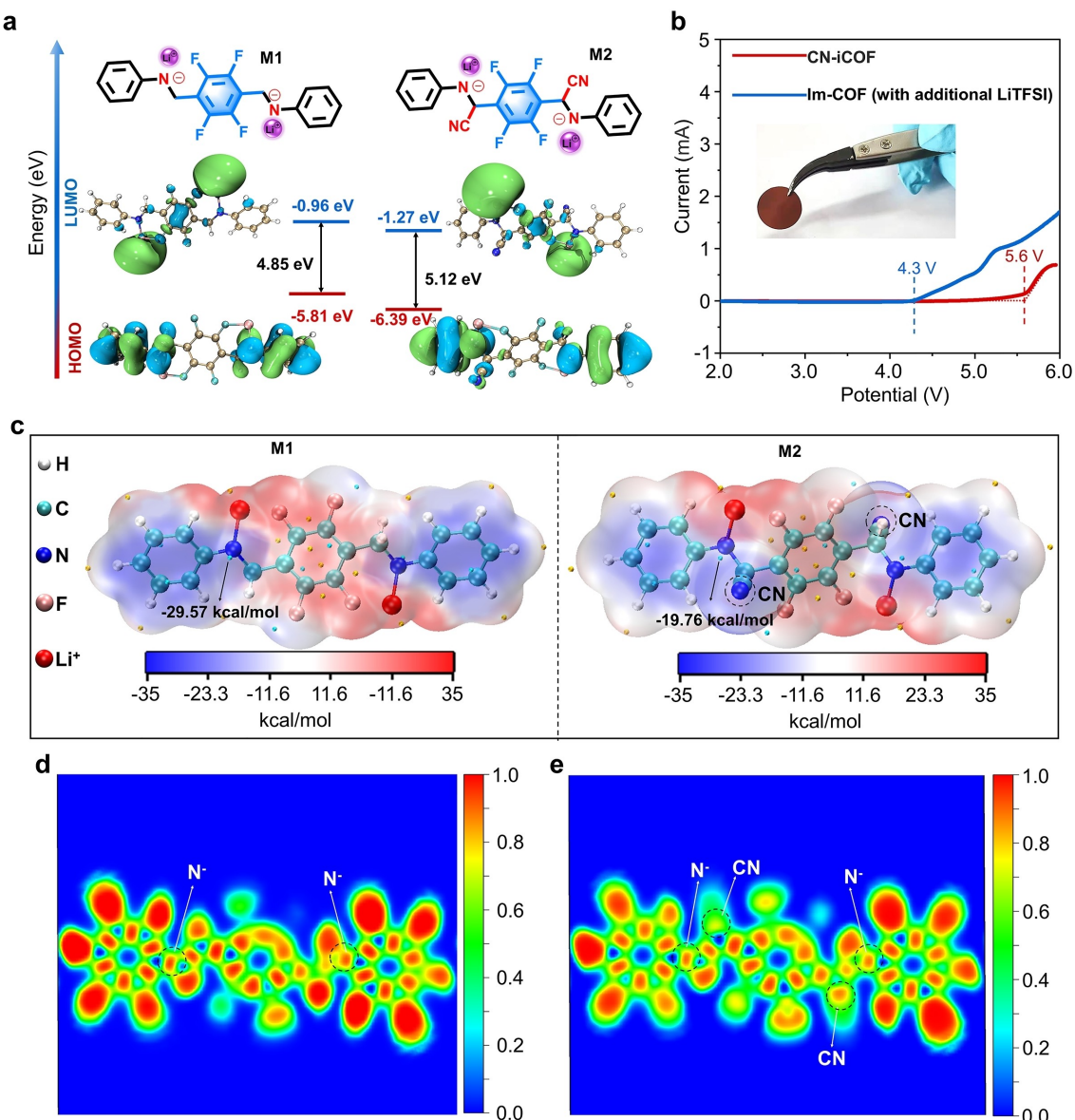


Figure 3. a) Optimized structure and calculation of HOMO/LOMO energies of iCOF molecular structure segment of M1 (without nitrile groups) and M2 (with nitrile groups) by DFT. b) LSV curves comparing between Im-COF (with additional LiTFSI) and CN-iCOF SSE at 1 mVs⁻¹ at room temperature. Inset: image of self-standing CN-iCOF pellet. c) The optimized geometric configurations and electrostatic potential of M1 and M2 (cyan dots represent the minimum and yellow dots represent the maximum). d) Electron localization function of M1 and M2.

whereas Im-COF started to decompose at around 4.3 V. This experimental observation aligns with theoretical evidence, as well as previous report on the high-voltage benign property of polyacrylonitrile electrolytes,^[19] supporting that introduction of nitrile groups could notably widen the electrochemical window and providing a promising structural motif to enhance the anodic stability of electrolyte materials.

Besides the high-voltage compatibility, the difficult dissociation of Li⁺ ions from the clustered anionic centers owing to strong electrostatic interactions has been a known problem to improve conductivity for single-ion electrolytes.^[12a] In our studies, the nitrile groups were found also able to delocalize the negative charge from the azanide

anions and weaken the interaction with Li⁺ ions. To probe the domains in CN-iCOF framework that offer coordinating sites to Li⁺ ions, electrostatic potential (ESP) was calculated by DFT calculations. As illustrated in Figure 3c, the negative charge maxima (blue area) resided around the negatively charged N⁻ (-29.57 kcal/mol) when lack of nitrile groups, suggesting strong electrostatic interactions with Li⁺ ions. As nitrile groups were integrated, the electron density was dramatically pulled off from N⁻ (-19.76 kcal/mol) in azanide, which not only agrees well with previous reports that polar -CN groups with high electron density can coordinate with Li⁺ and participate in ion migration,^[20] but also contribute to delocalization of charge on anions. This finding was supported by the reduced binding energy

between Li^+ and M2 (-14.80 vs. -15.68 eV in $\text{Li}^+ \text{-M2}$) calculated by DTF in Figure S13. To further illustrate that the introduction of nitrile groups facilitated the dissociation of lithium ions, electronic localization function (ELF) maps were calculated to study the electron localization distribution at the azanide sites. The ELF value at the N^- site on the M2 fragment was observed to be lower than that at the corresponding N^- site on the M1 fragment, indicating that the incorporation of nitrile groups has resulted in electron delocalization at the azanide site.

Uniquely, beyond endowing oxidative stability and facilitated Li^+ dissociation, the design of nitrile groups on the tetrahedral sp^3 -carbon allowed their contorted alignment from the aromatic framework planes, which could serve as transport “ladders” along the one-dimensional anionic channels given the coordinating ability of $-\text{CN}$ to Li^+ , enhancing ion migration between the vertically stacked frameworks. To understand the distinctive ion conduction phenomenon in CN-iCOF fundamentally, we employed DFT to illuminate the Li^+ migration pathways and barriers within the channels. The migration of Li^+ inside the pores via the axial direction was previously revealed to constitute the main transport pathways of COF materials as electrolytes,^[11b,21] and was analyzed by investigating the transition states (TS) and their migration barriers (E_m) as Li^+ ions transport between the initial and final states (IS and FS, respectively). Notably, when the polar and Li^+ -binding nitrile groups were incorporated on the sp^3 -carbon adjacent to anionic center, they aligned along the axial migration pathway of Li^+ ions because of the tetrahedral geometry, thus acting as stepping “ladders” of Li^+ ions between the anionic centers. Such alignment reduced hopping gap between the frameworks (Figure 4a). Therefore, the migration barrier in M2 segment with nitrile groups was found to be much lower than that in M1 without nitriles (4.38 kcal/mol vs. 8.99 kcal/mol, Figure 4b), evidencing that benefitted from the presence of nitrile groups, Li^+ could readily detach from the framework and migrate along the pores, providing energetically favorable transport pathway and improving ionic transport in CN-iCOF (Figure S14). The “ladder” function of nitrile groups was also demonstrated by In situ FT-IR spectroscopy (Figure S15). When CN-iCOF material was charged at different voltages varied from 3.0 V to 4.5 V, the typical $-\text{CN}$ peaks gradually shifted from 2256 cm^{-1} to 2240 cm^{-1} , indicating that the nitrile groups participate the coordination with Li ions at higher voltages. The facilitated ion transport in CN-iCOF framework was further investigated using molecular dynamics (MD) to better understand the coordination environment and transport behavior of Li^+ ions. As the intrinsic feature of single-ion electrolyte, no additional lithium salt was needed and all Li^+ ions were counter-ions against the immobilized anions on the COF backbone. After equilibrium, the MD simulations captured snapshots of the typical distribution and transport pathways of Li^+ ions in CN-iCOF. The Li^+ migration path in the one-dimensional pore channels was monitored over 5 ns by MD (Figure 4c). Representative structures showed that Li^+ mainly distributed around the azanide nitrogen, nitrile groups, and

fluorine atoms within the CN-iCOF framework, as illustrated in Figure 4d. Among the binding sites, the average distance of $\text{Li}^+ \text{-CN}$ and $\text{Li}^+ \text{-N}^-$ is 1.93 \AA and 1.79 \AA , respectively, shorter than that of $\text{Li}^+ \text{-F}$ (2.07 \AA). This indicates stronger coordination of Li^+ with the anions and nitrile groups, while only weak binding between F functional group and Li^+ was observed.^[22] Moreover, the radial distribution functions (RDFs) shown in Figure 4e has shown that coordination number between azanide anion to Li^+ in CN-iCOF was approximately 3.0, which is higher than that of CN groups at 1.0 and F group at 0.5, evidencing the stronger competitive coordination of nitrile groups.

Next, solid electrolyte membranes with a diameter of 15 mm were prepared using cold-pressing method, resulting in solid-state electrolytes with dense morphology. As shown in Figure 5a, Following Gaussian fitting, the Young's modulus reached as high as 9.6 GPa , considerably surpassing that of Im-COF (4.2 GPa) and CN-COF (6.8 GPa , Figure S16). Dry CN-iCOF without any solvent residues attained a high ionic conductivity of $1.33 \times 10^{-5}\text{ S cm}^{-1}$ at 30°C and $3.46 \times 10^{-5}\text{ S cm}^{-1}$ at 70°C , which is outstanding given that all anions are immobilized. The enhanced Li^+ transport in the COF matrix was further supported by the high Li^+ diffusion coefficient of $1.54 \times 10^{-9}\text{ cm}^2\text{s}^{-1}$, as tracked by the slope of mean-squared displacement (MSD) in MD (Figure S17). In the absence of nitrile groups, the ionic conductivity of Im-COF was an order of magnitude lower at $1.08 \times 10^{-6}\text{ S cm}^{-1}$ (Figure S18), verifying that introduction of nitrile groups weakened the interactions between ion pairs and could help improve ionic conductivity. In addition, the ionic conductivity was measured as a function of temperature from 30 to 80°C using electrochemical impedance spectroscopy (EIS, Figure 5b). Fitting with Arrhenius equation yielded a low activation energy (E_a) of 0.20 eV , while E_a of Im-COF was found higher at 0.26 eV (Figure 5c). To assess the capability of CN-iCOF electrolyte to effectively transport lithium ions as a fraction of all mobile ions, Li^+ transference number was measured to be 0.93 via Bruce-Vincent-Evans method, representing a remarkable value among reported single-ion COFs (Figure 5d and Figure S19). The highly efficient Li^+ transport of CN-iCOF is among the best values achieved (Table S5), which could minimize transport polarization-induced dendrite growth as well as voltage deviation.^[23] As a comparison, the non-single ion analogue Im-COF showed considerably reduced t_{Li^+} of 0.57, which is comparable to other neutral COF systems and is higher than conventional polymer electrolytes, ascribed to the beneficial pore structures that could block transport of bulky anions.

Stable lithium electrodeposition is crucial for sustained long-term battery operation, and was evaluated by Li plating-stripping experiment in symmetric Li cells at ambient temperature. To enhance the physical contact between the solid COF material and electrodes, a limited drop of propylene carbonate (PC, $10\text{ }\mu\text{L}$, 20 wt %) possessing high boiling point and better safety was added facilitating interfacial ionic conduction for battery cycling (Figure S20–S21).^[11a] As shown in Figure 6a, the assembled $\text{Li} \parallel \text{CN-iCOF} \parallel \text{Li}$ battery maintained stable charge-discharge

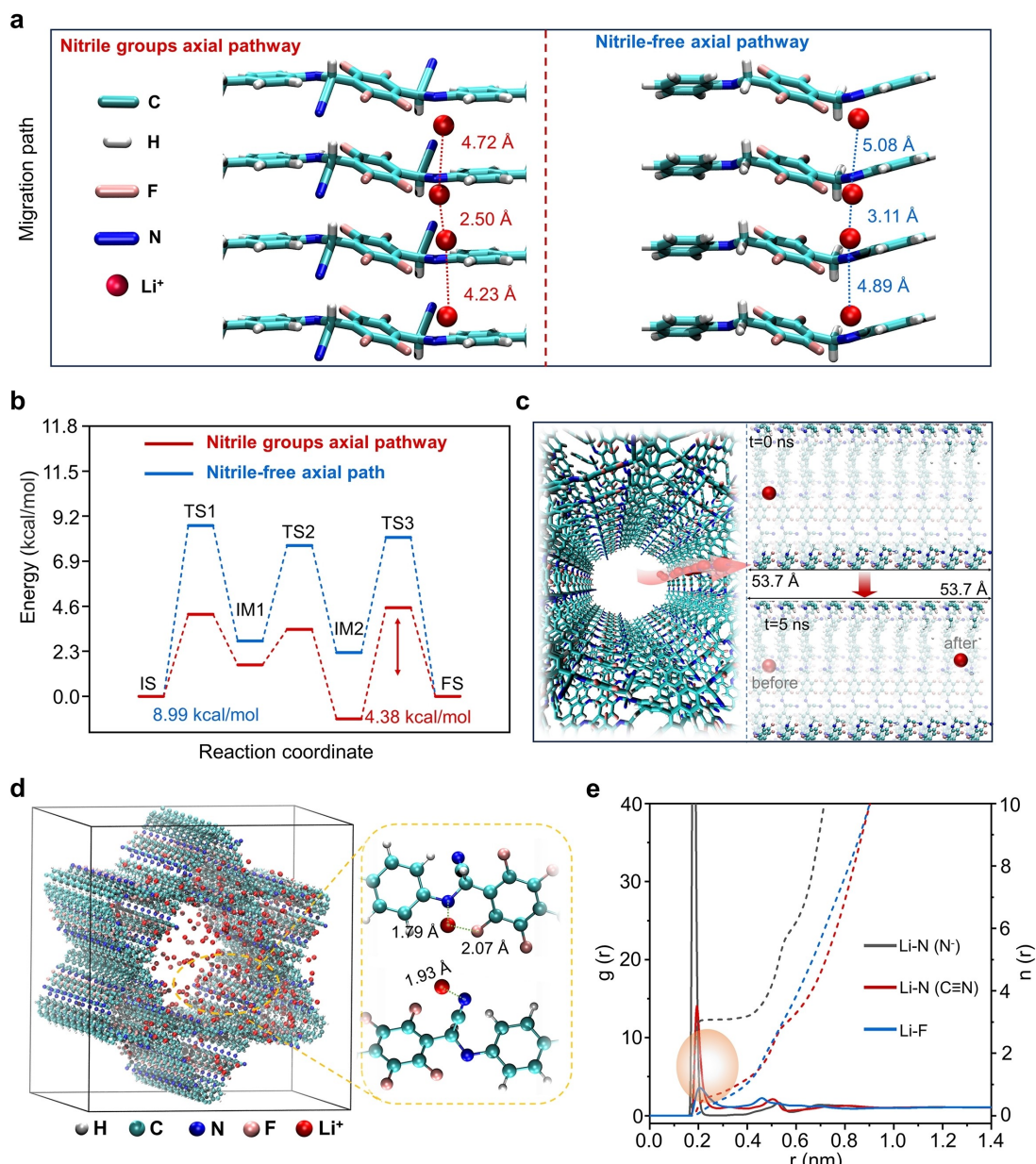


Figure 4. Theoretical elucidation of Li-ion migration behavior inside the pore. a) The hopping distance of lithium ions in axial pathways with or without nitrile groups. b) Li-ion migration correlation energy diagram. The initial, intermediate, and final states are abbreviated as IS, IM, and FS, respectively. c) One-dimensional migration channels of CN–iCOF, and MD snap-shots of Li^+ transport in CN–iCOF in 5 ns. d) Distance between Li^+ and N^- , CN and F^- by MD simulations, respectively, in representative local structures. (e) RDFs of Li^+ in the CN–iCOF.

for more than 1,100 h at a current density of 0.1 mA cm^{-2} and a lower degree of overpotential (100 mV), demonstrating structural stability of electrolytes and mitigation of lithium dendrites proliferation (Figure S22–26). In sharp contrast, Im-COF led to unstable plating and stripping behavior, and abrupt short-circuit after 200 h, attributed to unstable flux of Li^+ induced by worse polarization. Meanwhile, the CN–iCOF also demonstrated stable cycling performance at a current density of 0.2 mA cm^{-2} , lasting for 1,600 h (Figure S27). To investigate the practicability of CN–iCOF in high-voltage LMBs, $\text{Li}||\text{CN-iCOF}||\text{LCO}$ (LiCoO_2) cells were subsequently assembled to investigate

the galvanostatic charge–discharge cycling performance in full cells. Owing to the high conductivity and wide electrochemical window, ambient-temperature LMB battery operation was allowed at 30°C . Typical charge–discharge voltage profiles were plotted in Figure 6b, showing stable potential plateaus without polarization over 3.0 to 4.3 V. To further demonstrate that CN–iCOF can support high-voltage batteries and work with high-potential cathodes such as NCM811, $\text{Li}||\text{CN-iCOF}||\text{NCM811}$ cells were assembled and cycled from 3.0 to 4.5 V. As demonstrated in Figure 6c, CN–iCOF for the first time enabled reversible battery cycling up to 4.5 V based on single-ion COF electrolyte,

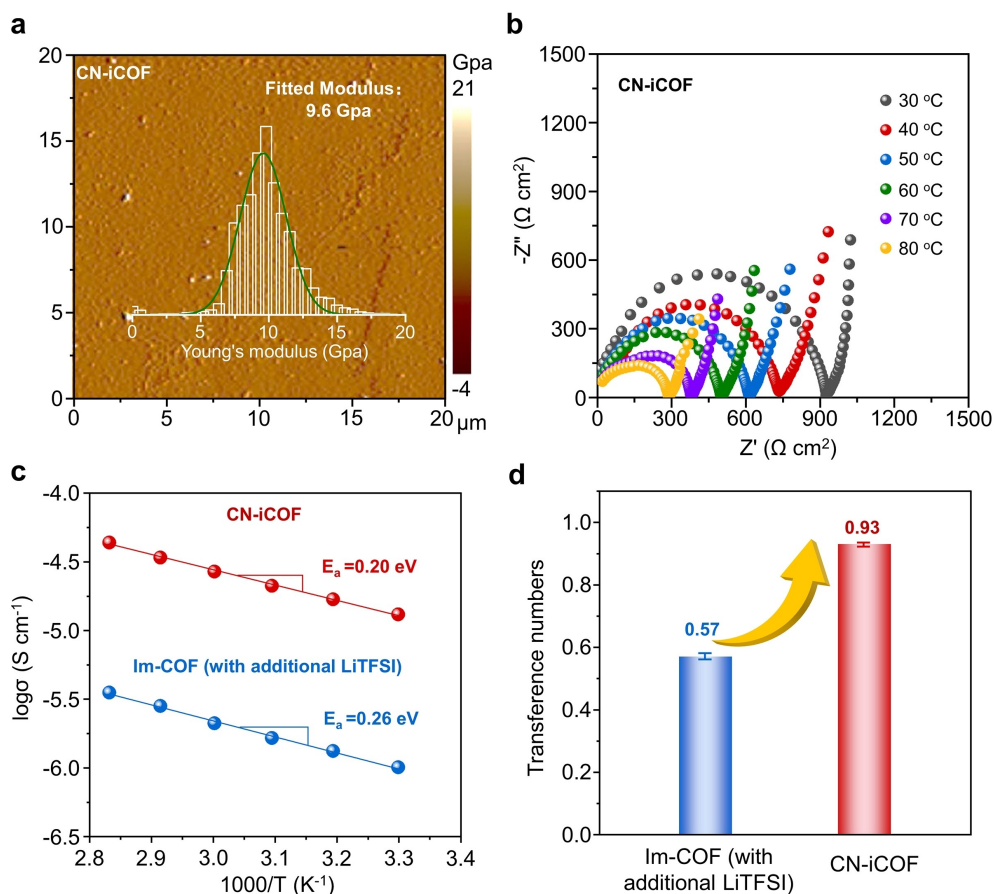


Figure 5. a) Force mapping and Young's modulus of the CN–iCOF at room temperature. b) Nyquist plots of electrochemical impedance spectroscopy (EIS) measurements over a range of temperatures. c) The temperature-dependent activation energy of CN–iCOF and Im-COF (with additional LiTFSI) fitted by Arrhenius equation. d) Li⁺ transference number (mean \pm s.d. of three independent replicates) of CN–iCOF and Im-COF (with additional LiTFSI) at room temperature.

showing limited polarization during charge–discharge cycles (Figure S28). The initial capacity was 176 mAh g⁻¹, and remained at 147 mAh g⁻¹ after 40 cycles, resulting in a capacity retention of 83 %. In contrast, the Li||Im-COF (with additional LiTFSI)||NCM811 battery assembled under the same conditions fail to work at all at such high voltages because Im-COF contains unstable imine bonds.^[7c] Rate capability was demonstrated (Figure S29) and the cycling evaluations of the CN–iCOF in Figure 6d showed that an initial capacity of 160 mAh g⁻¹ at a current rate of 0.1 C (Figure S30) as well as 0.05 C. After 130 cycles, the capacity remained at 101 mAh g⁻¹ with an average coulombic efficiency (CE) of 99 %. As a comparison, Im-COF displayed inferior and unsteady coulombic efficiency, showing an initial capacity of 63 mAh g⁻¹ under the same testing conditions (Figure S31).

Conclusion

In summary, we have synthesized a new single-ion covalent organic framework based on azanide anionic center, which showed high Li⁺ transport and high-voltage tolerance

simultaneously. Structural characterizations confirmed the designed COF structure with integrated nitrile functionality and successful lithiation. Both theoretical simulations and experimental investigations demonstrated that the electron-withdrawing nitrile groups not only reduced the HOMO value and widened the electrochemical window, but also facilitated the detachment of lithium ions from the iCOF framework and forms transport “ladders” based on the tetrahedral geometry of sp³-carbon adjacent to anionic centers. These synergistic effects contributed to the excellent electrochemical stability (5.6 V vs. Li⁺/Li) and Li⁺ conduction of CN–iCOF without any additives ($\sigma = 1.33 \times 10^{-5} \text{ S cm}^{-1}$, $t_{\text{Li}^+} = 0.93$, $E_a = 0.20 \text{ eV}$). When the CN–iCOF was assembled in Li-metal batteries, excellent performance including stable Li electrodeposition and reversible high-voltage battery cycling up to 4.5 V was achieved at ambient temperature. This new type of single-ion covalent organic framework containing nitrile groups offers a fresh strategy for the design of solid-state electrolytes.

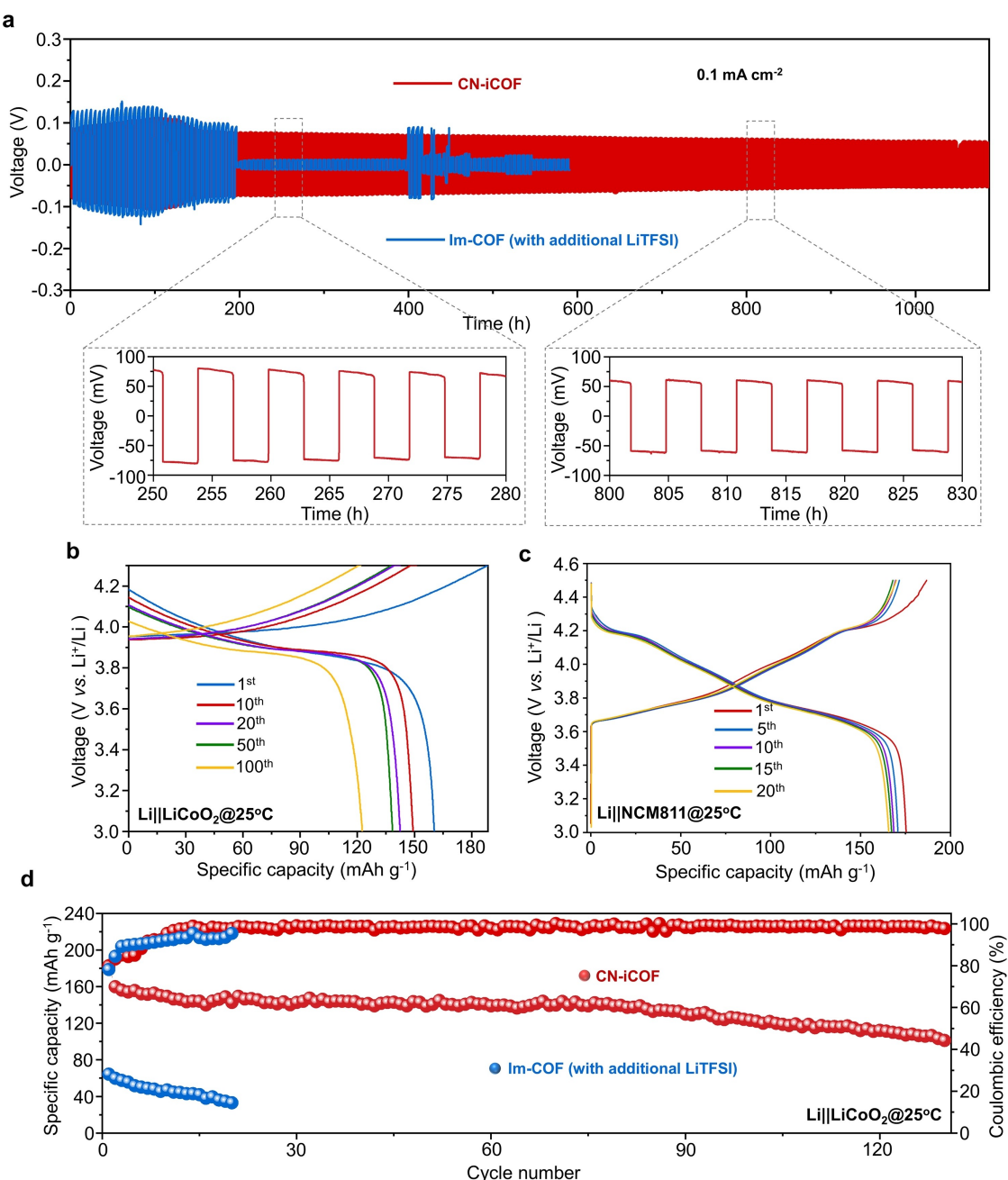


Figure 6. a) Galvanostatic cycling at a current density of 0.1 mA cm^{-2} in $\text{Li} \parallel \text{Li}$ symmetric cells with CN-iCOF and Im-COF (with additional LiTFSI). b) $\text{Li} \parallel \text{LCO}$ full-cell performance charged to 4.3 V with CN-iCOF at 25°C and C-rate of 0.05 C. c) $\text{Li} \parallel \text{NCM811}$ full-cell performance charged to 4.5 V with CN-iCOF at 25°C and C-rate of 0.05 C. d) Cycling in $\text{Li} \parallel \text{LCO}$ cells charged to 4.3 V with CN-iCOF at 25°C and C-rate of 0.05 C.

Acknowledgements

This research was financially supported by National Natural Science Foundation of China (22065037), Yunnan Fundamental Research Projects (202201AW070015, 202301AT070205) and Duke Kunshan University.

Conflict of Interest

The authors declare no conflict of interest.

Data Availability Statement

The data that support the findings of this study are available in the supplementary material of this article.

Keywords: single-ion covalent organic framework · high-voltage · cyanation · lithium batteries · solid-state electrolytes

- [1] M. Armand, J. M. Tarascon, *Nature* **2008**, *451*, 652–657.
- [2] a) W. Xu, J. Wang, F. Ding, X. Chen, E. Nasybulin, Y. Zhang, J.-G. Zhang, *Energy Environ. Sci.* **2014**, *7*, 513–537; b) D. Lin, Y. Liu, Y. Cui, *Nat. Nanotechnol.* **2017**, *12*, 194–206; c) L. Yu, S. Chen, H. Lee, L. Zhang, M. H. Engelhard, Q. Li, S. Jiao, J. Liu, W. Xu, J.-G. Zhang, *ACS Energy Lett.* **2018**, *3*, 2059–2067.
- [3] a) Q. Zhao, S. Stalin, C.-Z. Zhao, L. A. Archer, *Nat. Rev. Mater.* **2020**, *5*, 229–252; b) R. Chen, Q. Li, X. Yu, L. Chen, H. Li, *Chem. Rev.* **2020**, *120*, 6820–6877.
- [4] P. Albertus, V. Anandan, C. Ban, N. Balsara, I. Belharouak, J. Bueettner-Garrett, Z. Chen, C. Daniel, M. Doeffer, N. J. Dudney, B. Dunn, S. J. Harris, S. Herle, E. Herbert, S. Kalnauš, J. A. Libera, D. Lu, S. Martin, B. D. McCloskey, M. T. McDowell, Y. S. Meng, J. Nanda, J. Sakamoto, E. C. Self, S. Tepavcevic, E. Wachsman, C. Wang, A. S. Westover, J. Xiao, T. Yersak, *ACS Energy Lett.* **2021**, *6*, 1399–1404.
- [5] S. Xia, X. Wu, Z. Zhang, Y. Cui, W. Liu, *Chem* **2019**, *5*, 753–785.
- [6] a) V. Bocharova, A. P. Sokolov, *Macromolecules* **2020**, *53*, 4141–4157; b) J. C. Bachman, S. Muy, A. Grimaud, H.-H. Chang, N. Pour, S. F. Lux, O. Paschos, F. Maglia, S. Lupart, P. Lamp, L. Giordano, Y. Shao-Horn, *Chem. Rev.* **2016**, *116*, 140–162.
- [7] a) Z. Li, H. Zhang, X. Sun, Y. Yang, *ACS Energy Lett.* **2020**, *5*, 3244–3253; b) H. Sun, X. Xie, Q. Huang, Z. Wang, K. Chen, X. Li, J. Gao, Y. Li, H. Li, J. Qiu, W. Zhou, *Angew. Chem. Int. Ed.* **2021**, *60*, 18335–18343; c) C. Niu, W. Luo, C. Dai, C. Yu, Y. Xu, *Angew. Chem. Int. Ed.* **2021**, *60*, 24915–24923.
- [8] a) K. Geng, T. He, R. Liu, S. Dalapati, K. T. Tan, Z. Li, S. Tao, Y. Gong, Q. Jiang, D. Jiang, *Chem. Rev.* **2020**, *120*, 8814–8933; b) J. Li, X. Jing, Q. Li, S. Li, X. Gao, X. Feng, B. Wang, *Chem. Soc. Rev.* **2020**, *49*, 3565–3604; c) W. Li, W. Xie, F. Shao, J. Qian, S. Han, P. Wen, J. Lin, M. Chen, X. Lin, *Chem* **2023**, *9*, 117–129; d) Y. Zhu, Q. Bai, S. Ouyang, Y. Jin, W. Zhang, *ChemSusChem* **2024**, *17*, e202301118; e) Y. Hu, L. J. Wayment, C. Haslam, X. Yang, S.-h. Lee, Y. Jin, W. Zhang, *EnergyChem* **2021**, *3*, 100048.
- [9] H. Zhang, C. Li, M. Piszczyk, E. Coya, T. Rojo, L. M. Rodriguez-Martinez, M. Armand, Z. Zhou, *Chem. Soc. Rev.* **2017**, *46*, 797–815.
- [10] a) B. Qiao, G. M. Leverick, W. Zhao, A. H. Flood, J. A. Johnson, Y. Shao-Horn, *J. Am. Chem. Soc.* **2018**, *140*, 10932–10936; b) H. Chen, H. Tu, C. Hu, Y. Liu, D. Dong, Y. Sun, Y. Dai, S. Wang, H. Qian, Z. Lin, L. Chen, *J. Am. Chem. Soc.* **2018**, *140*, 896–899.
- [11] a) Y. Hu, N. Dunlap, S. Wan, S. Lu, S. Huang, I. Sellinger, M. Ortiz, Y. Jin, S.-h. Lee, W. Zhang, *J. Am. Chem. Soc.* **2019**, *141*, 7518–7525; b) K. Jeong, S. Park, G. Y. Jung, S. H. Kim, Y.-H. Lee, S. K. Kwak, S.-Y. Lee, *J. Am. Chem. Soc.* **2019**, *141*, 5880–5885; c) Y. Du, H. Yang, J. M. Whiteley, S. Wan, Y. Jin, S.-H. Lee, W. Zhang, *Angew. Chem. Int. Ed.* **2016**, *55*, 1737–1741; d) Y. Hu, N. Dunlap, H. Long, H. Chen, J. Wayment Lacey, M. Ortiz, Y. Jin, A. Nijamudheen, L. Mendoza-Cortes Jose, S.-h. Lee, W. Zhang, *CCS Chem.* **2021**, *3*, 2762–2770.
- [12] a) S. Han, P. Wen, H. Wang, Y. Zhou, Y. Gu, L. Zhang, Y. Shao-Horn, X. Lin, M. Chen, *Nat. Mater.* **2023**, *22*, 1515–1522;
- b) R. Bouchet, S. Maria, R. Meziane, A. Aboulaich, L. Lienafa, J.-P. Bonnet, T. N. T. Phan, D. Bertin, D. Gigmes, D. Devaux, R. Denoyel, M. Armand, *Nat. Mater.* **2013**, *12*, 452–457; c) J. Huang, L. Cheng, Z. Zhang, C. Li, K.-T. Bang, A. Liem, H. Luo, C. Hu, Y. M. Lee, Y. Lu, Y. Wang, Y. Kim, *Adv. Energy Mater.* **2024**, *n/a*, 2400762; d) X. Liang, Y. Tian, Y. Yuan, Y. Kim, *Adv. Mater.* **2021**, *33*, 2105647.
- [13] S. S. Park, Y. Tulchinsky, M. Dincă, *J. Am. Chem. Soc.* **2017**, *139*, 13260–13263.
- [14] a) Q. Xu, S. Tao, Q. Jiang, D. Jiang, *Angew. Chem. Int. Ed.* **2020**, *59*, 4557–4563; b) J.-H. Lee, H. Lee, J. Lee, T. W. Kang, J. H. Park, J.-H. Shin, H. Lee, D. Majhi, S. U. Lee, J.-H. Kim, *ACS Nano* **2023**, *17*, 17372–17382.
- [15] X.-T. Li, J. Zou, T.-H. Wang, H.-C. Ma, G.-J. Chen, Y.-B. Dong, *J. Am. Chem. Soc.* **2020**, *142*, 6521–6526.
- [16] a) N. von Aspern, G. V. Röschenthaler, M. Winter, I. Cekic-Laskovic, *Angew. Chem. Int. Ed.* **2019**, *58*, 15978–16000; b) X. Wang, C. Zhang, M. Sawczyk, J. Sun, Q. Yuan, F. Chen, T. C. Mendes, P. C. Howlett, C. Fu, Y. Wang, X. Tan, D. J. Searles, P. Král, C. J. Hawker, A. K. Whittaker, M. Forsyth, *Nat. Mater.* **2022**, *21*, 1057–1065; c) Z. Yu, H. Wang, X. Kong, W. Huang, Y. Tsao, D. G. Mackanic, K. Wang, X. Wang, W. Huang, S. Choudhury, Y. Zheng, C. V. Amanchukwu, S. T. Hung, Y. Ma, E. G. Lomeli, J. Qin, Y. Cui, Z. Bao, *Nat. Energy* **2020**, *5*, 526–533; d) C. Xiao, X. Liu, W. Li, X. Ma, J. Qian, X. Lin, *Batteries & Supercaps* **2024**, *n/a*, e202400078; e) M. Ma, F. Shao, P. Wen, K. Chen, J. Li, Y. Zhou, Y. Liu, M. Jia, M. Chen, X. Lin, *ACS Energy Lett.* **2021**, *6*, 4255–4264.
- [17] Q. Guan, L.-L. Zhou, Y.-B. Dong, *J. Am. Chem. Soc.* **2023**, *145*, 1475–1496.
- [18] a) Y. Peng, L. Li, C. Zhu, B. Chen, M. Zhao, Z. Zhang, Z. Lai, X. Zhang, C. Tan, Y. Han, Y. Zhu, H. Zhang, *J. Am. Chem. Soc.* **2020**, *142*, 13162–13169; b) T.-Y. Zhou, S.-Q. Xu, Q. Wen, Z.-F. Pang, X. Zhao, *J. Am. Chem. Soc.* **2014**, *136*, 15885–15888.
- [19] S. Xiao, L. Ren, W. Liu, L. Zhang, Q. Wang, *Energy Storage Mater.* **2023**, *63*, 102970.
- [20] a) W. Li, P. Wen, Y. Ren, W. Xie, J. Lin, M. Chen, Y. Yang, X. Lin, *ACS Energy Lett.* **2023**, *8*, 5128–5135; b) Y. Yamada, K. Furukawa, K. Sodeyama, K. Kikuchi, M. Yaegashi, Y. Tateyama, A. Yamada, *J. Am. Chem. Soc.* **2014**, *136*, 5039–5046.
- [21] G. Zhao, Z. Mei, L. Duan, Q. An, Y. Yang, C. Zhang, X. Tan, H. Guo, *Carbon Energy* **2023**, *5*, e248.
- [22] M. Jia, P. Wen, Z. Wang, Y. Zhao, Y. Liu, J. Lin, M. Chen, X. Lin, *Adv. Funct. Mater.* **2021**, *31*, 2101736.
- [23] a) M. Cui, Y. Qin, Z. Li, H. Zhao, L. Liu, Z. Jiang, Z. Cao, J. Zhao, B. Mao, W. Yu, Y. Su, R. Vasant Kumar, S. Ding, Z. Qu, K. Xi, *Sci. Bull.* **2024**, *69*, 1706–1715; b) Z. Sun, K. Xi, J. Chen, A. Abdelkader, M.-Y. Li, Y. Qin, Y. Lin, Q. Jiang, Y.-Q. Su, R. Vasant Kumar, S. Ding, *Nat. Commun.* **2022**, *13*, 3209.

Manuscript received: June 2, 2024

Accepted manuscript online: July 30, 2024

Version of record online: September 13, 2024